IOP PUBLISHING PHYSICS IN MEDICINE AND BIOLOGY

Phys. Med. Biol. **54** (2009) 2901–2914 doi:10.1088/0031-9155/54/9/021

Experimental evaluation of a robust optimization method for IMRT of moving targets

Christian Vrančić[1], Alexei Trofimov[2], Timothy C Y Chan[3], Gregory C Sharp[2] and Thomas Bortfeld[2]

[1] Department of Radiation Oncology, Mannheim Medical Center, University of Heidelberg, Mannheim, Germany
[2] Department of Radiation Oncology, Massachusetts General Hospital and Harvard Medical School, Boston, MA 02114, USA
[3] Operations Research Center, Massachusetts Institute of Technology, Cambridge, MA 02139, USA

E-mail: cvrancic@ix.urz.uni-heidelberg.de

Received 5 October 2008, in final form 25 March 2009
Published 21 April 2009
Online at stacks.iop.org/PMB/54/2901

Abstract

Internal organ motion during radiation therapy, if not considered appropriately in the planning process, has been shown to reduce target coverage and increase the dose to healthy tissues. Standard planning approaches, which use safety margins to handle intrafractional movement of the tumor, are typically designed based on the maximum amplitude of motion, and are often overly conservative. Comparable coverage and reduced dose to healthy organs appear achievable with robust motion-adaptive treatment planning, which considers the expected probability distribution of the average target position and the uncertainty of its realization during treatment delivery. A dosimetric test of a robust optimization method for IMRT was performed, using patient breathing data. External marker motion data acquired from respiratory-gated radiotherapy patients were used to build and test the framework for robust optimization. The motion trajectories recorded during radiation treatment itself are not strictly necessary to generate the initial version of a robust treatment plan, but can be used to adapt the plan during the course of treatment. Single-field IMRT plans were optimized to deliver a uniform dose to a rectangular area. During delivery on a linear accelerator, a computer-driven motion phantom reproduced the patients' breathing patterns and a two-dimensional ionization detector array measured the dose delivered. The dose distributions from robust-optimized plans were compared to those from standard plans, which used a margin expansion. Dosimetric tests confirmed the improved sparing of the non-target area with robust planning, which was achieved without compromising the target coverage. The maximum dose in robust plans did not exceed 110% of the prescription, while the minimum target doses were comparable in standard and robust plans. In test courses, optimized for a simplified target geometry,

and delivered to a phantom that moved in one dimension with an average amplitude of 17 mm, the robust treatment design produced a reduction of more than 12% of the integral dose to non-target areas, compared to the standard plan using 10 mm margin expansion.

(Some figures in this article are in colour only in the electronic version)

1. Introduction

Current standard treatment planning for lung in radiation therapy mitigates the effects of motion by adding safety margins to the clinical target volume (CTV) (e.g., ICRU 92 1999, Bradley *et al* 2007, Lilenbaum *et al* 2008). The internal target volume (ITV) margins are typically chosen to accommodate the maximum expected amplitude, regardless of other characteristics and parameters of motion. However, in a realistic respiratory trajectory, the probability of finding the tumor in the deep inhalation, exhalation or mid-ventilation position varies both fraction to fraction and intrafractionally. For instance, in many patients, the probability of finding the tumor in the exhalation phase is higher than for the inhale. This type of additional information about the motion can be utilized in the design of a treatment plan. (Recipes for planning margin reduction have been proposed, e.g., based on target dosage probabilities estimated from patient-population statistics (Wolthaus *et al* 2008).)

The experimental work presented here deals with the aspects of a treatment planning approach that employs realistic probability density functions (PDFs) in the design of treatment plans. More specifically, it makes use of the probability of a particular displacement of the target as well as the underlying uncertainties in a patient's breathing pattern. This framework of a PDF-based robust optimization methodology was proposed and developed by Chan *et al* (2006). Accounting for the uncertainties of the PDF realization is the main new feature that distinguishes this approach from other published probability-based planning methods, the performance of which is heavily reliant on high stability and reproducibility of internal motion patterns (Unkelbach and Oelfke 2004, Trofimov *et al* 2005, Chu *et al* 2005). Specifically, this approach aims to design uncertainty bounds that would likely contain the realized PDF, and thus make the result robust against the commonly observed variations in the breathing pattern. The set-up uncertainties can as well be accommodated within such bounds. Recently, several methods have been proposed that employ the concept of robust optimization to reduce the effect of set-up errors (Ólafsson and Wright 2006, Pflugfelder *et al* 2008) and uncertainties in tumor control and tissue complication probabilities (Witte *et al* 2007).

Probability-based planning is by no means the only manner in which the motion effects in radiotherapy can be mitigated. Other approaches to handle the uncertainties due to intrafractional movement were proposed or are currently in clinical use: gated treatment (Berson *et al* 2004), breath-hold techniques (Remouchamps *et al* 2003), as well as tracking with robotic systems (Nioutsikou *et al* 2008), stereotactic beams (Casamassima *et al* 2006), dynamic multi-leaf collimators (Keall *et al* 2005) or couch position corrections (D'Souza *et al* 2005). All of them aim to reduce the effective motion amplitude. Consequently, the dose delivered to the healthy tissue is reduced. This is achieved either by tracking the tumor directly, often in combination with the use of prediction models, or by selectively delivering the dose only to specific phases of the breathing cycle.

The robust planning method that was investigated in this study makes use of both the prediction model and selectivity aspects. Uncertainty sets, which are used to model the expected variability of motion, are built from patient data. At the same time, some

of the probability distributions with low or negligible likelihood of realization are excluded in the optimization process (e.g., the unlikely case that the tumor would spend almost all of the time at the full exhale position, etc).

The application of the model of Chan *et al* to a case of lung tumor, in a treatment planning exercise, demonstrated an appreciable dose reduction to healthy tissue, compared to standard plans that used margin expansion (Bortfeld *et al* 2008). However, this result was achieved in the assumption that the effects of fractionation and interplay between the target and the multi-leaf collimator (MLC) motion were negligible in both plans. This assumption was motivated by, among others, the results of Bortfeld *et al* (2002) who examined the impact of the interplay and showed that the effect of intrafractional movement is relatively small, and is further reduced with fractionation.

The purpose of this study was to investigate the effects of fractionation and to validate, in a realistic delivery environment, the design of the uncertainty bounds and the assumptions in regards to the MLC interplay. In this paper, the robust model on which this work is based is briefly introduced, followed by the presentation of the methods and results of the dosimetric study that compares robust-optimized plans with a standard safety-margin-based plan.

2. Methods

2.1. Model of uncertainty

The basic tenet of the approach of Chan *et al* (2006) is that one cannot expect a patient to breathe consistently and reproducibly during multiple fractions of the therapy course, and even within a single treatment fraction. Nevertheless, one can reasonably expect that the basic structure of the breathing waveform will retain a certain degree of stability throughout the treatment, and therefore can be parametrized on average (Neicu *et al* 2003). Further, it is assumed that the deviation from such an average pattern can be described with an uncertainty model particular to a patient or a class of patients. Investigations in respiratory physiology documented the fact that variability in free breathing patterns is generally not random (Benchetrit 2000).

The robust approach requires the construction of PDFs from the target motion information to describe the likelihood of a specific displacement of the tumor. Such information can be obtained from direct observation of the tumor or via surrogate markers (Gierga *et al* 2005, Hoisak *et al* 2004). At our institution, Massachusetts General Hospital, respiratory traces are routinely recorded with a real-time position management system (Varian Medical Systems, Inc., Palo Alto, CA) during respiratory-gated treatments (Berbeco *et al* 2005).

For the robust planning formulation, the uncertainties for each discrete displacement were defined by adding error bars around a specific 'nominal' PDF that reflects the motion information known (or assumed) *a priori*. The nominal PDF can be obtained pre-treatment, for example, during the acquisition of respiratory-correlated CT (4D-CT) data (which is routinely administered at many hospitals to patients with lung or liver tumors) or during treatment simulation. If sufficient data are available before the treatment, one can use the variations within the patient's data (e.g., sampling and analyzing segments of a long trace, as in figure 1) to design bounds around the nominal PDF.

An alternative is to use the data from other patients with similar breathing patterns to approximate intra- and interfractional variations of the PDF (Trofimov *et al* 2008, Bortfeld *et al* 2008). The scale of variations, or the width of designed uncertainty bounds based on the data from a cohort of patients, can be adjusted to best fit the specific individual. In this study, the second option was used, and assumed that it is possible to estimate probabilistic variations from a class of patients with similar breathing patterns.

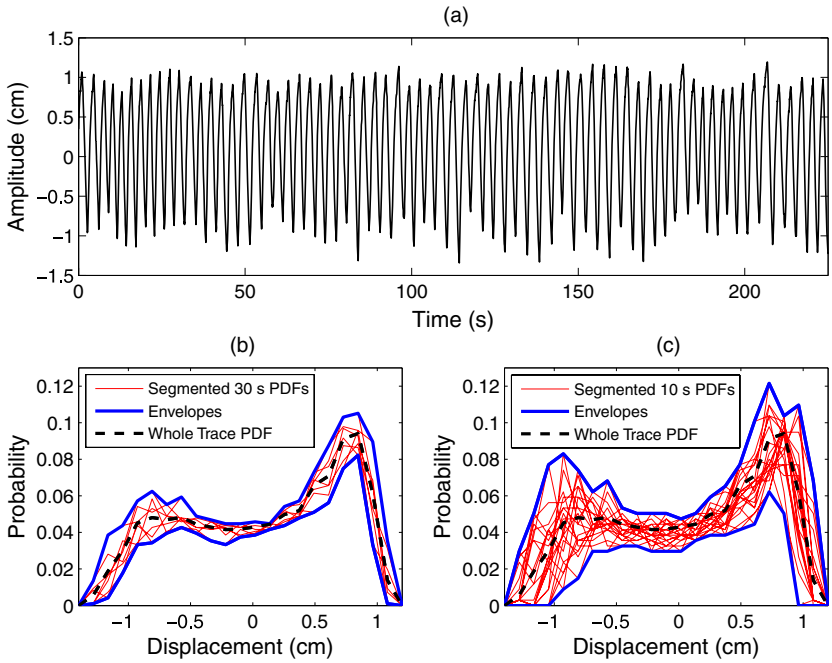

Figure 1. (a) A sample respiratory trace, the corresponding PDF and intrafractional variability bounds constructed from consecutive (b) 30 s long segments and (c) 10 s long segments of the trace. The width of the data bins is 1 mm.

Table 1. Summary of motion data used in this study.

Patient	Tumor site	Number of traces	Purpose
A	Lung	75	Define uncertainty set
B	Lung	53	Define uncertainty set
C	Mediastinum	79	Define uncertainty set
D	Liver	44	Define uncertainty set
E	Mediastinum	78	Test of model (37 fractions)
F	Liver	56	Test of model (15 fractions)

The anonymized data from six randomly selected patients (labeled A through F) were divided into two subsets, as shown in table 1. One subset was used to build the motion uncertainty model and the other to test the optimized plans. The uncertainty bounds were built from full-trace PDFs of patients A–D and then applied to single (nominal) PDFs of patients E and F. This is meant to approximate a situation in which the uncertainty framework is needed for a patient for whom the available respiration data are limited (e.g., only one trace is available for patients E and F), while some prior data exist from a *class* of patients (A–D) and is used to predict the variability bounds. Figure 1 illustrates how an uncertainty set can be built from a single motion trace, by segmenting and sampling. The first trace of patient A was chosen as the source of the nominal PDF: it had an average amplitude of motion of 17 mm and a maximum amplitude of 20 mm. The error bars were determined based on the maximum and minimum probability values for a particular displacement from all four patients. For this purpose, the PDFs from all traces were scaled to the average amplitude of the nominal trace:

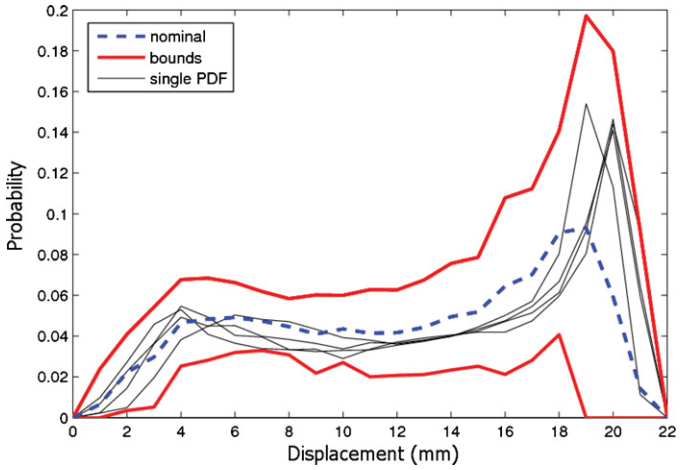

Figure 2. Robust uncertainty set of probability distribution functions exhibiting the bowl-shaped form, typical of a breathing pattern with an emphasized exhalation phase of the cycle. The dashed blue PDF is the reference trace (pre-treatment) and the bold red lines are the error bars.

17 mm. The PDF envelopes were built to yield the maximal and minimal values and, by that, the variation range for each displacement. The variability bounds equal to half of the total variability range were then applied to the nominal PDF. Thus, the total range was the same as in the uncertainty set, with the variability band centered around the nominal PDF. Since it is not known *a priori* whether or not the nominal PDF represents an outlier case, the assumption is that the same bounds apply above and below the nominal PDF, i.e., there is equal probability of local motion undersampling and oversampling. The negative values in lower PDF bounds were reset to zero. An example of such an error set is shown in figure 2.

Ideally, the resulting uncertainty set will accommodate any kind of respiratory-related target displacement during the irradiation. In other words, all realized PDFs are expected to lie within the uncertainty bounds. However, this approach still produces acceptable results even if the realized PDF lies slightly outside the set. For this reason, construction of the uncertainty set should consider the stability of the breathing pattern of a particular patient, and the PDF variability bounds estimated from a cohort of patients may be scaled, i.e., expanded or shrunk accordingly.

2.2. *Plan optimization*

The objective of robust optimization in the formulation of Chan *et al* (2006) is to minimize the total integral dose to patient, subject to the tumor receiving the required dose, for all motion realization scenarios consistent with the uncertainty model. The mathematical formulation of the robust approach is

$$\text{minimize} \sum_{v\in\mathcal{V}}\sum_{b\in\mathcal{B}}\sum_{x\in\mathcal{X}} D_{v,x,b}\,p(x)\,w_{\mathrm{b}}$$

$$\text{subject to} \sum_{b\in\mathcal{B}}\sum_{x\in\mathcal{X}} D_{v,x,b}\,\widetilde{p}(x)\,w_{\mathrm{b}} \geqslant \Theta_{\mathrm{v}} \qquad \forall\, v \in \text{Target}, \quad \forall\, \widetilde{p}(x) \in \text{Uncertainty set}, \tag{1}$$

where $\widetilde{p}(x)$ represents any single PDF from the uncertainty set, all contained within the uncertainty bounds constructed around the nominal PDF $p(x)$, which can be realized during

the individual treatment fractions. The term $D_{v,x,b}$ in equation (1) is the shift-differentiated dose influence matrix whose elements represent the dose delivered by a unit-weight beamlet b, to a voxel v, for a displacement x, from its initial position. This matrix is multiplied with the non-negative beamlet weights, $w_b \geqslant 0$, and the probability $p(x)$ of finding the voxel at a certain position, to obtain the actual dose delivered. Ideally, the dose in any target voxel should not be below the prescription value Θ_v. The beamlet weights w_b are the optimized parameters in this formulation.

For the margin formulation, the probability for all displacements is assumed to be equally likely. This makes the margin solution very robust with respect to the variability in the motion pattern (as long as the amplitude of motion does not exceed the margin width). On the other hand, the margin solution protects against many extremely unlikely scenarios, for instance a δ-function for a stationary tumor at any position within the margins is among the acceptable realized PDFs. The trade-off for this high and, arguably, excessive degree of robustness is the higher dose delivered to surrounding healthy tissues, which are included in the internal target volume (Bortfeld *et al* 2008).

The problem formulation for the margin approach is

$$\begin{aligned} &\text{minimize} \sum_{v\in\mathcal{V}} \sum_{b\in\mathcal{B}} \sum_{x\in\mathcal{X}} D_{v,x,b}\, p(x)\, w_b \\ &\text{subject to} \sum_{b\in\mathcal{B}} D_{v,x,b} w_b \geqslant \Theta_v \qquad \forall\, v \in \text{Target}, \quad \forall\, x \in \text{Displacements}. \end{aligned} \tag{2}$$

This formulation ensures that all target voxels are sufficiently covered for all acceptable displacements x, regardless of their relative probability. This is manifested in equation (2) being independent of the realized motion PDF $\widetilde{p}(x)$. As stated above, any δ-function PDF, $\widetilde{p}(x) = \delta(x)$, within the assumed margin would represent an acceptable motion pattern, and would not lead to a reduction of the tumor dosage. Thus, the upper bound of the uncertainty range for $\widetilde{p}(x)$ is implicitly equal to 1 for all displacements, incorporating all possible movement scenarios.

For dosimetric tests, sample plans were optimized, using the software package CPLEX 9 (ILOG SA, France). The target volume was defined as a rectangle of 8 cm (x) by 10 cm (y). The movement was assumed in the x-direction with a mean amplitude of 17 mm, which resulted in a maximal amplitude of 20 mm for the nominal trace, but allowed for larger amplitudes for the realized traces. For the margin plan, the 1 cm planning target expansion was applied only in the direction of motion (x). Uniform dose distributions were optimized on a grid with a resolution of 1×1 mm ^{2}. Dose calculation and optimization were performed for a single depth of 10 cm of water. The dose deposit from 5×5 mm ^{2} pencil beams was modeled based on the measurements performed during commissioning of the clinical linear accelerator used for tests (a Clinac 2100, with a 120-leaf MLC by Varian Medical Systems, Palo Alto, CA). Optimized test intensity patterns were sequenced for delivery assuming 5 mm MLC-leaf resolution at the isocenter.

2.3. Experimental setup

The delivery setup is illustrated in figure 3. The fields were calibrated to deliver 180 cGy per fraction at the isocenter, at a depth of 10 cm of water-equivalent material, 90 cm SSD. Dose distributions were measured using a two-dimensional array consisting of 1020 single ionization chambers, spaced at 7.6 mm (ImRT MatrixX by Scanditronix Wellhofer, Bartlett, TN). The detector was placed on the top of a computer-controlled, motor-driven motion phantom, which reproduced realistic motion trajectories using the patient respiratory traces as an input.

Figure 3. Experimental setup for the dosimetric study: a commercial diode array was placed on the top platform of the motion phantom and covered with water-equivalent material with a total thickness of 10 cm. The linac gantry was at 0°.

The motion phantom was fed with traces from two patients (E and F in table 1). For simplicity, it was assumed that the mean amplitude of breathing would remain stable throughout the treatment course. The reference amplitude was adopted from the nominal data set, the first respiratory trace of patient A. All traces were scaled to have a mean amplitude of 17 mm, from exhale to inhale. Furthermore, the low-frequency component within the trace (below 25 mHz) was removed with a band-pass filter in order to eliminate the respiratory baseline drifts within the motion traces as proposed by Trofimov *et al* (2008). The drifts can be more appropriately corrected mechanically, e.g., with treatment couch position correction (D'Souza *et al* 2005), because of their slow-changing nature, rather than with robust optimization methods. Removing the drifts from the motion data helps to reduce the variability bounds.

3. Results

3.1. Continuum of robust solutions and test plan selection

Before discussing the dosimetric results of delivery of robust-optimized plans, it is worthwhile to briefly describe the effect of the choice of the uncertainty bounds in the model on the form of the robust solution. As mentioned above, the uncertainty bounds may be constructed based on the data from a patient population, and subsequently used to appropriately model the expected variability of motion for the patient for whom the robust treatment plan is being designed. These bounds may either be transferred to the patient-specific nominal PDF $p(x)$, without adjustment ('100% scaling'), or rescaled to better match the motion variability characteristics of a given patient.

Figure 4 illustrates the effect of the definition of the uncertainty set on the results of robust optimization. The optimized intensity maps are shown for a range of scaling factors applied

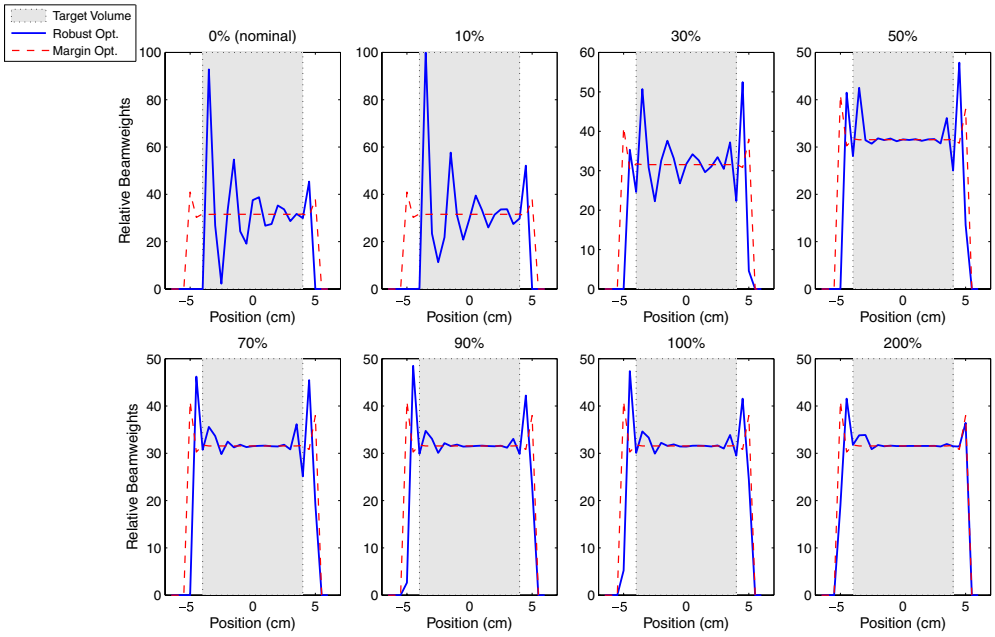

Figure 4. Continuum of robust optimization solutions. Intensity maps optimized assuming various scaling of the uncertainty bounds. Top row, left to right: 0, 10, 30 and 50% scaling; bottom row: 70, 90, 100, 200% scaling. The margin-plan solution is plotted as the dashed line, for comparison. *y*-axes were scaled to the rounded maximum of the relative beamlet weights.

to the uncertainty bounds, for a number of values between 0 and 100%, and also 200%. In the context of patients' breathing, a shrinking of the bounds (scaling of below 100%) corresponds to a more stable breathing pattern with less uncertainty. The result of optimization is a plan, which allows for a smaller variance of the realized PDF, but spares more healthy tissue if the realized PDFs lie within the modeled bounds. The '0% scaling', at the extreme, collapses the bounds onto the nominal case, i.e. allows for no deviation from the nominal PDF. Thus, any variation may result in an undesired dose deposit.

Expanding the bounds and allowing for greater variation in motion result in a gradual decrease of the modulation in the intensity profile. Additionally, more intensity units (beamlets) that project close to the edges of the target get activated, widening the distribution. The larger the bounds get, the closer the outcome is to a margin solution where the field is expected to cover the rectangular area of 10×10 cm ^{2} (for the target width of 8 cm and 2 cm motion amplitude). In this case, a margin represents a nearly homogeneous beamlet weight distribution, except for two relatively small 'horns' at the border as a result of the intensity modulation optimization, to achieve a sharper penumbra. These segments of excess dose are expected to wash out while the target moves. However, they may still deliver a slightly higher dose at the inside rim of the target.

The optimized robust plan with 100% bounds (no scaling) was selected for delivery to the moving phantom. The intensity map is shown in figure 5.

Generally, the robust-optimized plans exhibit a higher grade of oscillation in the intensity map compared to margin plans, which may result in a higher number of MLC segments for delivery. The test plans were translated for dynamic delivery, with the leaf motion restricted to under 5 mm from segment to segment: the resulting number of MLC segments was 41 for the margin plan and 44 for the robust plans for both patients E and F. (Of note, with step-and-shoot

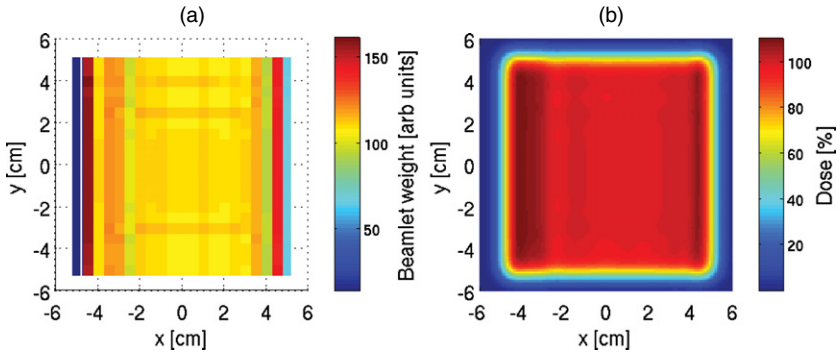

Figure 5. (a) The intensity map for the robust plan (100% bounds) and (b) the corresponding dose distribution (calculation for delivery to a static target).

segmentation and delivery, the margin plan would require only 7 segments, compared to 17 and 15, respectively, for plans E and F). Additionally, the dose 'horns' close to the rim of the target are higher for the robust plans, which increases the required number of monitor units (MUs). In the dosimetric study, approximately 46% more MUs were required for delivery of the robust plan for patient E (441 MUs) and 37% more for patient F (414 MUs), compared with the margin solution (302 MUs). For the tests, the dose delivery rate was 300 MU min $^{-1}$.

3.2. Dose measurements

The test plans were delivered in a simulation of a complete fractionated treatment, with the phantom moving according to the breathing traces of patients E and F (see table 1), which were not used in the design of the uncertainty set. Course E was delivered in 37 fractions and course F consisted of 15 fractions. The comparison of the cumulative dose delivered in the simulated course E, for the robust- and margin-optimized plans, is shown in figure 6.

Even though the robust outcomes of separate fractions showed discrepancies from the plan, due to the motion interplay, the total delivered dose converged to the expected value with only two horns inside the target remaining, which are characteristic of robust-optimized plans. The horns increase the dose within the tumor but help lowering the dose deposited in the healthy tissue. The reduction of the integral dose delivered outside of the target was 13% and 12%, in courses E and F, respectively. Compared to the outcome of a margin-optimized plan, this is achieved by reducing the weights of beamlets lying outside the static tumor frame and using the horns to wash out the dose toward the edges of the target, which move in and out of the irradiation field during delivery. The results of both courses were dosimetrically similar.

Figure 7 shows the fraction-by-fraction dynamics in the accumulated dose inhomogeneities for the course E. After approximately ten fractions, the deviation of the minimum value of the dose deposited ('cold spot') from the prescribed target dose becomes less than 2%, for both the margin- and the robust-optimized plans. On the other hand, the maximum dose values ('hot spots') are higher for the robust-optimized plan because of the presence of the beamlet intensity 'horns', as in figure 6.

A valid concern is that, due to the higher modulation in robust profiles, the desired dose profile conformity may not be achieved within the limited number of delivery fractions. Figure 8 compares the dynamics of the root mean square errors (RMSEs) of both plans as a function of the fraction number, where the different RMSEs are defined as

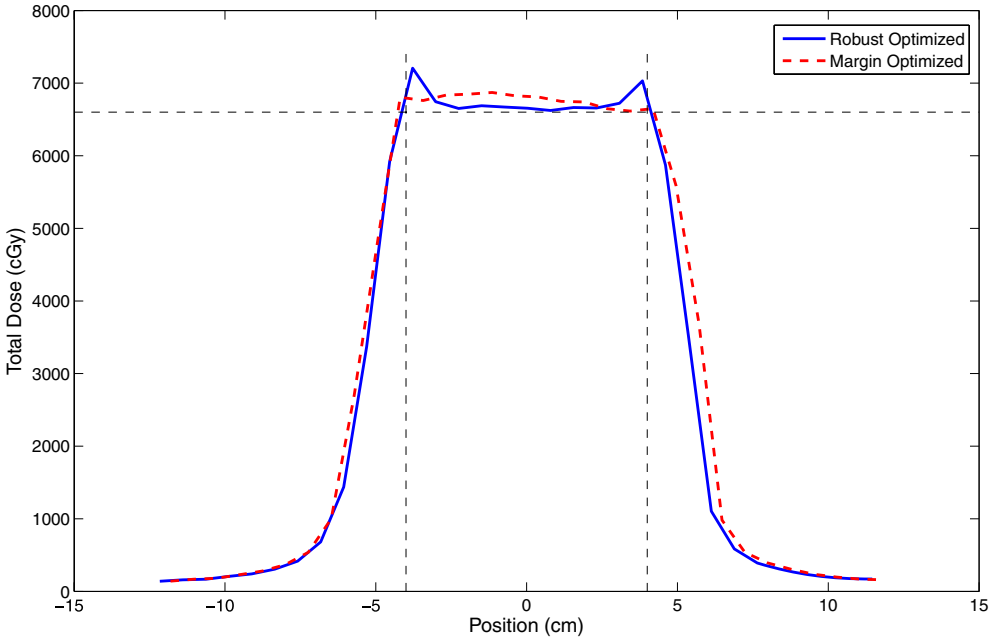

Figure 6. Cumulative dose profiles, along the direction of target motion, from robust- and margin-optimized plans, delivered in 37 fractions.

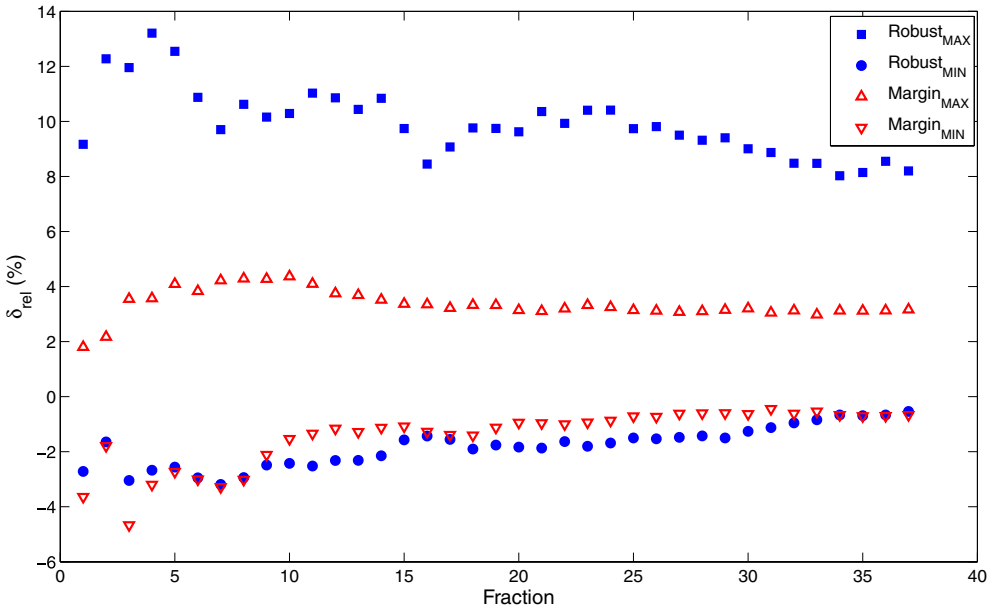

Figure 7. Relative size of the maximum and minimum values (hot and cold spots) of the deviation in the delivered dose from the prescription within the target volume, for robust- and margin-optimized plans, from the 37-fraction course E.

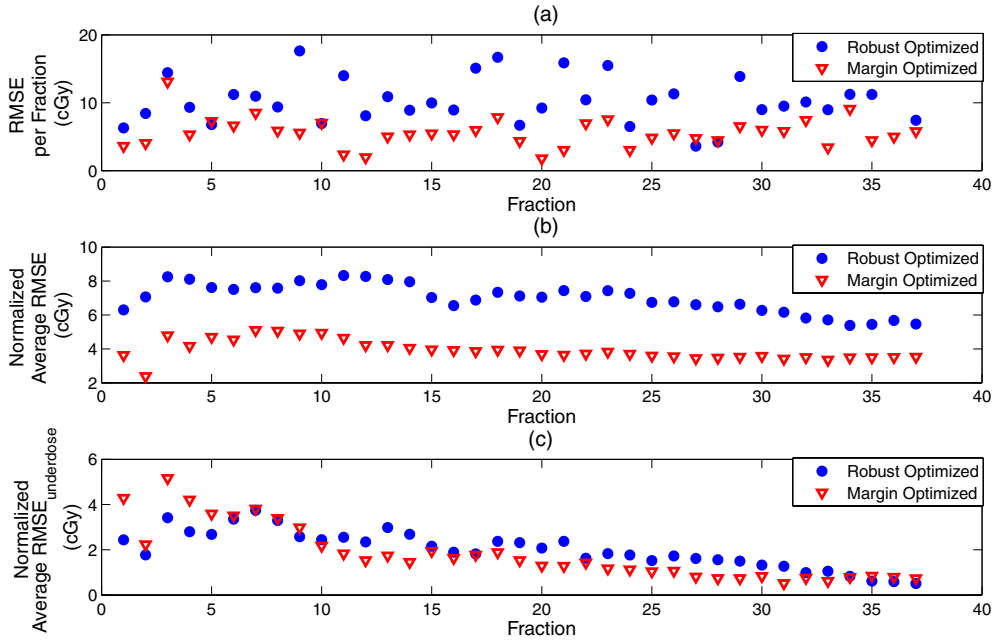

Figure 8. Root mean square dose error, as defined by equations (3) and (4), for robust and margin-optimized plans of the course E. Values are shown (a) for separate fractions, (b) accumulated after a given number of fractions. Plot (c) shows the size of accumulated underdosing or 'cold spots' separately.

$$\mathrm{RMSE}_{\mathrm{fraction}} = \sqrt{\sum_{v} \left(\Theta_v^{\mathrm{frac}} - d_v^{\mathrm{frac}}\right)^2} \tag{3}$$

and

$$\mathrm{RMSE}_{\mathrm{normalized}} = \frac{1}{n}\sqrt{\sum_{v} \left(n \cdot \Theta_v^{\mathrm{frac}} - d_v^{\mathrm{total}}\right)^2}, \tag{4}$$

where n is the number of fractions, Θ_v^{frac} is the prescribed, d_v^{frac} is the delivered dose in voxel v in a given fraction and $d_v^{\mathrm{total}} = \sum d_v^{\mathrm{frac}}$ is the total dose after n fractions. From figure 8, it is obvious that the longer the treatment goes, the smaller the total RMSE becomes in both cases. Notably, the RMSE of the robust-optimized plan remains 2–3 cGy larger for a fraction delivering 180 cGy to the tumor tissue. This difference is caused by the dose horns, as evident from figure 8(c), where only the deviation caused by underdosing is displayed, i.e., $d_v^{\mathrm{total}} < n \cdot \Theta_v^{\mathrm{frac}}$.

4. Discussion and conclusions

This dosimetric study aimed to test the validity of the theoretical construct of a robust optimization method of Chan *et al* (2006) in a realistic delivery environment. An important aspect, which would have been difficult to model in simulations, was the combination of intrafractional variations of the breathing traces collected from radiotherapy patients and MLC-based IMRT delivery, to investigate the effect of motion interplay.

The interplay arises from the fact that each MLC segment, or aperture, from the beginning of the field to the end will sample a different probability distribution of the position of the moving tumor. Consequently, different parts of the target are exposed to the radiation for different amounts of time. This means that the 'whole-trace' PDF will be sampled only partially by individual target voxels. This can be illustrated by cutting the breathing trace into smaller segments and building the PDFs separately, as visualized in figure 1, for two different lengths of the sampled trace segments. It is obvious that the shorter the time scales, the larger the variations from the whole-trace PDF will result. The robust framework is able to accommodate such variations in a sampled PDF for individual MLC segments. Thus, if the uncertainty bounds are transferred from the patient population data, the choice of the scaling factor needs to be made based on the expected exposure per MLC segment.

As illustrated in figure 4, modulation in the optimized intensity maps increases with the reduced variability bounds, as the uncertainty set approaches the single 'nominal' PDF. One of the aims of this study was to confirm that this increased modulation in the delivered dose per fraction will largely cancel out in a fractionated course. Figure 8 illustrates the dynamics of convergence of the delivered dose to the plan, in a realistic treatment environment, with the MLC-based IMRT delivered to a moving target. Similar robustness against 'cold spots' was observed between the robust- and margin-based plans. However, the robust plans reduced the integral dose outside the target by over 12% in both test courses. The 'horns' in the dose deposition for the robust-optimized plans should not be of concern, when taking into account that this overdosing of approximately 5–10% within the tumor helps to significantly reduce the dose delivered to the adjacent healthy tissue. The extent of such reduction depends on the amplitude of the motion, as well as on its stability and reproducibility. Nonetheless, the probability distribution and the robust model must be built carefully for every patient to ensure that the hot spots will not be placed within the healthy tissue.

The results observed in the tests are specific to the selected simplified target geometry within a homogeneous medium, delivery with a single beam and one-dimensional motion. The relative dosimetric advantage from delivery of robust-optimized plans may be affected by the amplitude of motion, the choice of planning margins as well as MLC resolution, sequencing parameters and algorithm. Due to the limited resolution of the ionization chamber array used for the measurements, point-by-point dose comparisons were avoided in favor of more generalized metrics, such as standard deviations between the values of delivered and expected doses over relatively large areas, and integral doses. Further, the correlation between the integral dose and the treatment risk predicators (such as, for the lung, the mean dose, the volumes receiving 10 or 20 Gy, i.e. V_{10} or V_{20}, etc) obviously vary from case to case, depending on the beam orientation, target position within the organ, size of margins, to name just a few factors.

The principal advantage of the robust approach is its general formulation and flexible character. It includes the margin solution as well as the nominal 'single-PDF' solution for a reproducible motion, as subsets. The robust optimization framework can be adjusted for each patient individually, depending on the stability of the patient's breathing pattern. The motivation for scaling the uncertainty bounds is to better tailor them to a specific patient with limited respiratory data available, e.g. scale up if a higher variability is expected than 'class average'. If necessary, the bounds can be shrunk to decrease the dose to the healthy tissue for patients with a very stable breathing. The validity of the assumptions about the stability of breathing patterns and uncertainty bound designs can be checked against the data acquired during treatment and corrected as needed.

Future research directions will focus on a harmonized and general approach to build the uncertainty set from restricted pre-treatment data of a patient. This information can be

combined with data from former patients with a similar degree of variability in the breathing. Therefore, criteria must be established to cluster the breathing data and ensure quality assurance as the benefit of this approach, and the progress within a treatment is monitored. This could be realized in an adaptive treatment course by monitoring the tumor motion and dose deposit during multiple fractions, and comparing the outcome with the planned uncertainty set, in order to be able to correct both the model and the dose prescription, if necessary (de la Zerda *et al* 2007, Webb and Bortfeld 2008).

Acknowledgments

This work was supported by the US National Cancer Institute under grant RO1-CA118200 and the United States-Israel Binational Science Foundation grant 2003275. CV was supported by Landestiftung Baden-Württemberg and the University of Heidelberg through the student practical training program. The authors thank Dr Steve B Jiang for assistance with the motion phantom.

References

Benchetrit G 2000 Breathing pattern in humans: diversity and individuality *Respir. Physiol.* **122** 123–9

Berbeco R I, Nishioka S, Shirato H, Chen G T and Jiang S B 2005 Residual motion of lung tumours in gated radiotherapy with external respiratory surrogates *Phys. Med. Biol.* **50** 3655–67

Berson A M, Emery R, Rodriguez L, Richards G, Ng T, Sanghavi S and Barsa J 2004 Clinical experience using respiratory gated radiation therapy: comparison of free-breathing and breath-hold techniques *Int. J. Radiat. Oncol. Biol. Phys.* **60** 419–26

Bortfeld T, Chan T C Y, Trofimov A and Tsitsiklis J N 2008 Robust management of motion uncertainty in intensity modulated radiation therapy *Oper. Res.* **56** 1461–73

Bortfeld T, Jokivarsi K, Goitein M, Kung J and Jiang S B 2002 Effects of intra-fraction motion on IMRT dose delivery: statistical analysis and simulation *Phys. Med. Biol.* **47** 2203–20

Bradley *et al* 2007 A randomized phase III comparison of standard-dose (60 Gy) versus high-dose (74 Gy) conformal radiotherapy with concurrent and consolidation Carboplatin/Paclitaxel ± Cetuximab (Ind #103444) in patients with stage IIIA/IIIB non-small cell lung cancer *Radiation Therapy Oncology Group (RTOG)* 0617

Casamassima F, Cavedon C, Francescon P, Stancanello J, Avanzo M, Cora S and Scalchi P 2006 Use of motion tracking in stereotactic body radiotherapy: evaluation of uncertainty in off-target dose distribution and optimization strategies *Acta Oncol.* **47** 943–7

Chan T C Y, Bortfeld T and Tsitsiklis J N 2006 A robust approach to IMRT optimization *Phys. Med. Biol.* **51** 2568–83

Chu M, Zinchenko Y, Henderson S G and Sharpe M B 2005 Robust optimization for intensity modulated radiation therapy treatment planning under uncertainty *Phys. Med. Biol.* **50** 5463–77

D'Souza W D, Naqvi S A and Yu C X 2005 Real-time intra-fraction-motion tracking using the treatment couch: a feasibility study *Phys. Med. Biol.* **50** 4021–33

de la Zerda A, Armbruster B and Xing L 2007 Formulating adaptive radiation therapy (ART) treatment planning into a closed-loop control framework. *Phys. Med. Biol.* **52** 4137–53

Gierga D P, Brewer J, Sharp G C, Betke M, Willett C G and Chen G T 2005 The correlation between internal and external markers for abdominal tumors: implications for respiratory gating *Int. J. Radiat. Oncol. Biol. Phys.* **61** 1551–8

Hoisak J D, Sixel K E, Tirona R, Cheung P C and Pignol J P 2004 Correlation of lung tumor motion with external surrogate indicators of respiration *Int. J. Radiat. Oncol. Biol. Phys.* **60** 1298–306

ICRU (Internation Commission on Radiation Units) 1999 *Prescribing, Recording and Reporting Photon Beam Therapy* (*Report 62*) (Bethesda, MD: ICRU)

Keall P J, Joshi S, Vedam S S, Siebers J V, Kini V R and Mohan R 2005 A comparison of beam characteristics for gated and nongated *Med. Phys.* **32** 942–51

Lilenbaum R *et al* 2008 A phase II trial of combined modality therapy with growth factor support for patients with limited stage small cell lung cancer *Radiation Therapy Oncology Group (RTOG)* 0623

Neicu T, Shirato H, Seppenwoolde Y and Jiang S B 2003 Synchronized moving aperture radiation therapy (SMART): average tumour trajectory for lung patients *Phys. Med. Biol.* **48** 587–98

Nioutsikou E, Seppenwoolde Y, Symonds-Tayler J R, Heijmen B, Evans P and Webb S 2008 Dosimetric investigation of lung tumor motion compensation with a robotic respiratory tracking system: an experimental study *Med. Phys.* **35** 1232–40

Ólafsson A and Wright S J 2006 Efficient schemes for robust IMRT treatment planning *Phys. Med. Biol.* **51** 5621–42

Pflugfelder D, Wilkens JJ and Oelfke U 2008 Worst case optimization: a method to account for uncertainties in the optimization of intensity modulated proton therapy *Phys. Med. Biol.* **53** 1689–700

Remouchamps V M, Letts N, Yan D, Vicini F A, Moreau M, Zielinski J A, Liang J, Kestin L L, Martinez A A and Wong J W 2003 Three-dimensional evaluation of intra- and interfraction immobilization of lung and chest wall using active breathing control: a reproducibility study with breast cancer patients *Int. J. Radiat. Oncol. Biol. Phys.* **57** 968–78

Trofimov A, Rietzel E, Lu H M, Martin B, Jiang S, Chen G T Y and Bortfeld T 2005 Temporo-spatial IMRT optimization: concepts, implementation and initial results *Phys. Med. Biol.* **50** 2779–98

Trofimov A, Vrancic C, Chan T C Y, Sharp G C and Bortfeld T 2008 Tumor trailing strategy for intensity-modulated radiation therapy of moving targets *Med. Phys.* **35** 1718–33

Unkelbach J and Oelfke U 2004 Inclusion of organ movements in IMRT treatment planning via inverse planning based on probability distributions *Phys. Med. Biol.* **49** 4005–29

Webb S and Bortfeld T 2008 A new way of adapting IMRT delivery fraction-by-fraction to cater for variable intrafraction motion *Phys. Med. Biol.* **53** 5177–91

Witte M G, van der Geer J, Schneider C, Lebesque J V, Alber M and van Herk M 2007 IMRT optimization including random and systematic geometric errors based on the expectation of TCP and NTCP *Med. Phys.* **34** 3544–55

Wolthaus J W, Sonke J J, van Herk M, Belderbos J S, Rossi M M, Lebesque J V and Damen E M 2008 Comparison of different strategies to use four-dimensional computed tomography in treatment planning for lung cancer patients. *Int. J. Radiat. Oncol. Biol. Phys.* **70** 1229–38